



Metallic cobalt microcrystals with flowerlike architectures: Synthesis, growth mechanism and magnetic properties

Run-Han Wang, Ji-Sen Jiang*, Ming Hu

Department of Physics, Center of Functional Nanomaterials and Devices, East China Normal University, Shanghai 200062, China

ARTICLE INFO

Article history:

Received 14 August 2008

Received in revised form 6 January 2009

Accepted 20 February 2009

Available online 6 March 2009

Keywords:

A. Metals

B. Chemical synthesis

B. Crystal growth

D. Microstructure

D. Magnetic properties

ABSTRACT

Well-defined, three-dimensional (3D) flowerlike metallic Co microcrystals with several radiating hexagonal-tapered petals assembled by particles size of 150–250 nm were fabricated via a facile hydrothermal reduction route under a fixed basic condition. The morphology and structure of the products were characterized by scanning electronic microscopy (SEM), energy-dispersive X-ray (EDX), transmission electron microscopy (TEM), selected area electron diffraction (SAED), X-ray photoelectron spectroscopy (XPS) and powder X-ray diffraction (XRD). The probable formation mechanism of the flowerlike Co microcrystals was discussed based on the experimental results. Magnetic properties of Co microcrystals were investigated by a commercial Physical Properties Measurement System (PPMS). The flowerlike products exhibited ferromagnetic characteristics with a saturation magnetization of 128.1 emu/g and a coercivity of 232.5 Oe at room temperature. Compared to the coercivity value of bulk Co, the products displayed a remarkable enhanced value due to their special morphology.

© 2009 Elsevier Ltd. All rights reserved.

1. Introduction

Morphological control of metals has become a subject of much intensive research due to its importance in fundamental scientific research and potential technological applications [1–4]. As one of the most important transition metals, cobalt displays a wealth of magnetic [5], electronic [6,7], optical [8], microwave [9] and catalytic [10] properties. Because the shape of the metal has significant influence on its properties, there has been an increasing number of reports on the synthesis of cobalt with various shapes, such as rods [11,12], chains [13,14], wires [15,16], belts [17], disks [18], platelets [19], tubes [20], and dendrites [21]. Meanwhile, the dependence between the shape and the properties of cobalt has been observed. For example, single-crystal Co nanoplatelets exhibit a distinct enhanced coercive force attributing to their 2D structures [22]. Self-assembled devices composed of periodic arrays of 10-nm-diameter cobalt nanocrystals display spin-dependent electron transport [6]. Therefore, if we can understand how to regulate the shape of metals, their chemical and physical properties may be tailored as desired.

Although materials with different morphologies have been prepared, selective synthesis of materials with novel morphologies always turns out to be a great challenge. To date, various synthetic methods such as electrochemical deposition [23], metal carbonyl

pyrolysis [24], and liquid-phase metal salt reduction [25] have been developed to fabricate cobalt. Among these methods, the metal carbonyl pyrolysis needs toxic or expensive precursors, and the reaction often performs at a high temperature, while the electrochemical deposition generally requires a complicated device and intricate processing. In the liquid-phase synthesis, capping molecules, micelles and complexing agents are usually applied to control the sizes and shapes of materials [14,17,26,27]. As one of the most common liquid-phase methods, the hydrothermal method is often used to prepare high purity materials, and to control the morphology of materials. Recently, hydrothermal method has been used to prepare Co. For instance, Xie et al. [17] prepared 1D single crystal hcp Co nanobelts by a hydrothermal reduction process at 160 °C. Liu et al. [28] reported a facile hydrothermal reduction route to fabricate highly ordered 2D snowflake-like Co microcrystals based on a precipitate slow-release controlled process. Li and Liao [29] synthesized 3D flowery Co microcrystals composed of several Co plates via a solvothermal route in which a water/ethanol mixture was used as a solvent and ethylenediamine tetraacetic acid sodium (EDTA) was introduced as a complexing agent, respectively.

In this work, we have synthesized three-dimensional flowerlike Co microcrystals in large quantities. The radiating hexagonal-tapered petals of the flowers were formed by assembly of Co particles sized of 150–250 nm. To the best of our knowledge, no reports for this unique morphology of metallic Co have been published up to the present. A formation mechanism of the 3D flowerlike Co microstructures was proposed based on the

* Corresponding author. Tel.: +86 21 62232001.

E-mail address: jsjiang@phy.ecnu.edu.cn (J.-S. Jiang).

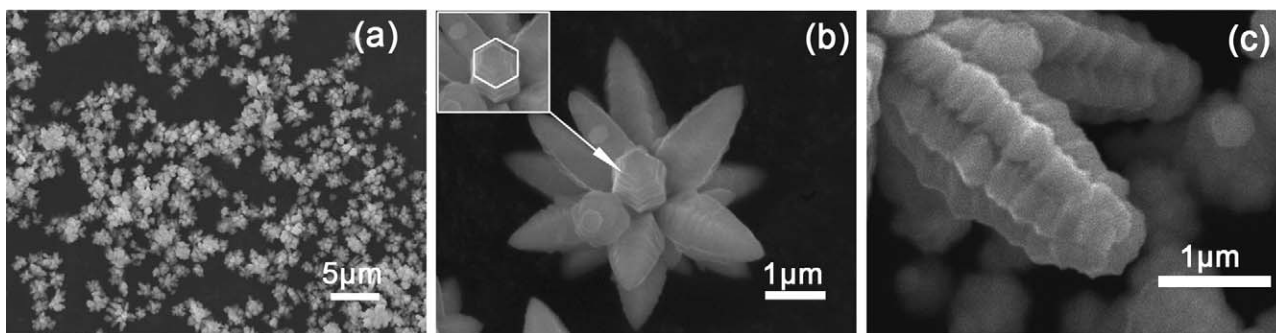


Fig. 1. (a) SEM image of the as-synthesized Co flowerlike microcrystals at 120 °C for 8 h. (b) An individual Co flowerlike microcrystal. (c) A single petal of the Co flowerlike microcrystal.

experimental observations. And the magnetic properties of the products were also investigated.

2. Experimental

2.1. Synthesis of flowerlike metallic Co microcrystals

All the reagents were of analytical grade and used without further purification. In a typical procedure, 0.2108 g of $\text{CoSO}_4 \cdot 7\text{H}_2\text{O}$, and 1 g of sodium citrate ($\text{Na}_3\text{C}_6\text{H}_5\text{O}_7 \cdot 2\text{H}_2\text{O}$) were dissolved in 30 mL of deionized water. 3 mL hydrazine hydrate ($\text{N}_2\text{H}_4 \cdot \text{H}_2\text{O}$, 85%) and 5 mL NaOH aqueous solution (1 M) were added dropwise into the above mixture while stirring. The final mixture was vigorously stirred for 30 min and then transferred into a 40 mL Teflon-lined stainless steel autoclave for hydrothermal treatment at 120 °C for 8 h. After the autoclave was cooled to room temperature naturally, the gray solid precipitation was then washed with distilled water and ethanol several times, and dried under vacuum at 50 °C for 10 h.

2.2. Characterization

The phase identification of the products was accomplished with powder X-ray diffraction (XRD) employing a Rigaku D/max 2550 X-ray diffractometer with $\text{Cu K}\alpha$ radiation ($\lambda = 1.5406 \text{ \AA}$). A scan rate of $0.02^\circ \text{ s}^{-1}$ was applied to record the pattern in the 2θ range of 30–80°. The scanning electron microscopy (SEM) images and energy-dispersive X-ray (EDX) analysis were obtained by using a JSM-6460 scanning electron microscope. X-ray photoelectron spectroscopy (XPS) measurement was carried out on a RBD upgraded PHI-5000C ESCA system (PerkinElmer). Transmission electron microscopy (TEM) images and the corresponding selected area electron diffraction (SAED) were collected with a JEM-2100F transmission

electron microscope at an accelerating voltage of 200 kV. Magnetic measurements for the samples were carried out at room temperature using a commercial Physical Properties Measurement System (PPMS, Quantum Design Inc.).

3. Results and discussion

The morphology of the as-prepared products formed at 120 °C for 8 h was examined by SEM. Typical SEM images of the products with different magnifications are given in Fig. 1. Fig. 1a shows the overall morphology of the sample, which indicates that the products mainly consist of flowerlike structures. The high-magnification image of a single Co flowerlike microcrystal shows that the 3D architecture is constituted by a few petals radiating from the center (Fig. 1b). Furthermore, each petal shows a hierarchical structure comprising a tapered trunk and many tight nanoparticles with size of 150–250 nm (Fig. 1c). The tight particles form a well-defined hexagon around the trunk (see inset in Fig. 1b).

The phase composition of the as-synthesized flowerlike products was characterized by XRD, and the XRD pattern of the sample is shown in Fig. 2a. The characteristic peaks of the as-prepared products arise at $2\theta = 41.68^\circ$, 44.50° , 47.46° , 62.80° and 75.91° , which have been assigned to (1 0 0), (0 0 2), (1 0 1), (1 0 2), and (1 1 0) planes respectively. All peaks of the products can be indexed as hexagonal close-packed (hcp) Co (JCPDS no. 05-0727). No peaks for impurities are detected indicating that the flowerlike microcrystals consist of pure metallic hcp cobalt. Additionally, the relative intensity of the peaks corresponding to the (0 0 2)/(1 0 1), (0 0 2)/(1 1 0) planes are remarkably higher than the standard values in JCPDS card, suggesting that the preferential crystal growth orientation of the product was in the [0 0 1] direction. EDX spectrum of the flowerlike products indicated that the sample is essentially pure Co (Fig. 2b). Only a very small amount of oxygen

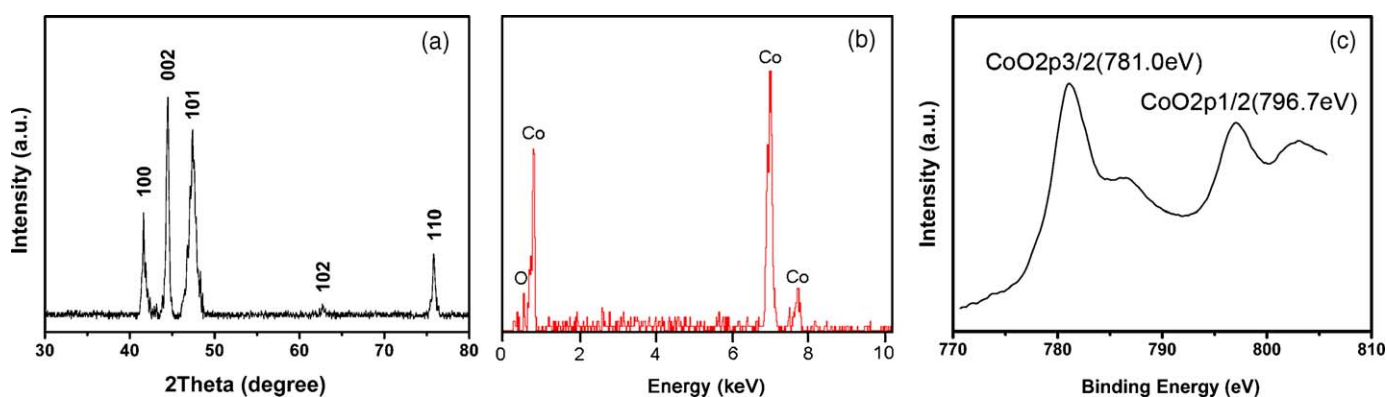


Fig. 2. XRD pattern (a), EDX spectrum (b), XPS spectrum of the as-synthesized flowerlike Co microcrystals at 120 °C for 8 h.

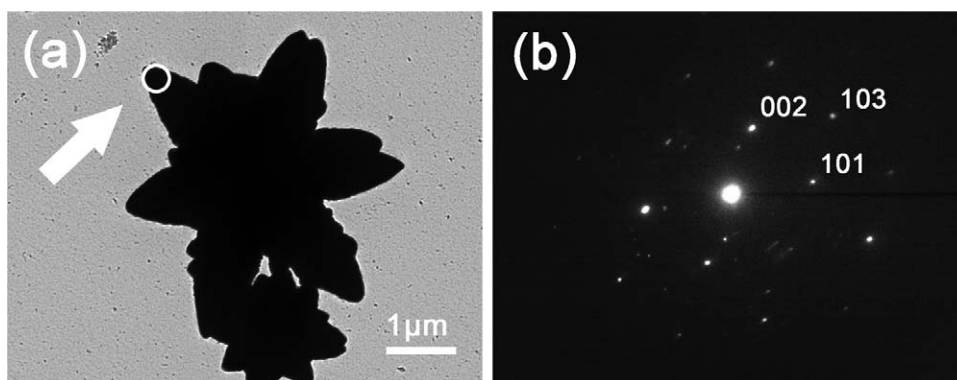


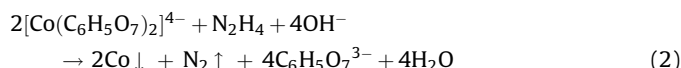
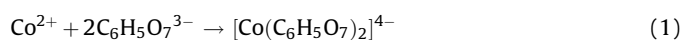
Fig. 3. (a) TEM image of flowerlike Co microcrystals. (b) The selected-area electron diffraction (SAED) pattern of the circled area in (a).

was detected, which was possibly from slight oxidation of the surface. The existence of CoO on the surface of the sample has been re-established on the basis of the binding energies of satellite peaks at 781.0 and 796.7 eV of CoO_{2p3/2} and CoO_{2p1/2}, respectively, found in the XPS spectrum (Fig. 2c) [30].

The morphology of the flowerlike Co was further determined by TEM as shown in Fig. 3a, which is consistent with that observed by SEM. Additionally, the sample shown in Fig. 3a was subjected to ultrasonication for 45 min before TEM analysis. It is noticeable that there is no obvious crack or destruction of the flowerlike Co after the ultrasonication, indicating a high stability of the product. Fig. 3b is a typical SAED pattern corresponding to the circled area in Fig. 3a. These pattern spots demonstrate the single-crystalline nature of this metallic Co microstructure. The interplanar spacings, obtained from the SAED pattern, are 2.034, 1.895, 1.142 Å which can be indexed to the (0 0 2), (1 0 1), and (1 0 3) planes of the hexagonal Co respectively. The SEAD pattern also confirms that the growth of the petals of the flowerlike Co single-crystal was along the [0 0 1] directions, which correspond to the (0 0 2) planes. It is in complete agreement with the XRD result.

The flowerlike Co superstructure obtained by the presented route has a micrometer and nanometer combined structure. It is widely accepted that this hierarchical structure is formed by the driving force of thermodynamics, because the supersaturated solution is not stable [31–33]. Such necessary thermodynamic nonequilibrium microenvironments can be easily achieved in wet chemical processes if complexing agents or surfactants are added into the reaction solutions. Therefore, it is supposed that the sodium citrate added into our reaction system plays an important role in the formation of the flowerlike Co microcrystals. To investigate the influence of sodium citrate on the formation of flowerlike Co microcrystals, contrast experiments were carried out at 120 °C for 8 h with different amount of sodium citrate. The SEM image of the prepared products shows that only irregular nanoparticle aggregations were formed in the absence of sodium citrate (Fig. 4a). When the amount of sodium citrate increased to 0.5 g, spherical particles and imperfect flowerlike particles were formed (Fig. 4b). We speculate that sodium citrate is mainly performing two tasks in this synthesis. Firstly, sodium citrate is used as a complexing agent. Citrate ions can coordinate with Co²⁺ ions to form stable complexing ions ([Co(C₆H₅O₇)₂]⁴⁻), which can decrease the concentration of free Co²⁺ ions in solution. As a result, the concentration of Co²⁺ ions is maintained at a stable level in the solution. After hydrazine hydrate (N₂H₄·H₂O), a potent reducing agent in alkali solution [34], is added into the solution, Co²⁺ ions are released slowly and reduced in hydrothermal condition, which leads to a relatively slow rate of generation of Co atoms. The chemical reaction can

be formulated as follows:



It is well accepted that a slow reaction rate was favorable for separating the growth step from the nucleation step, which is in

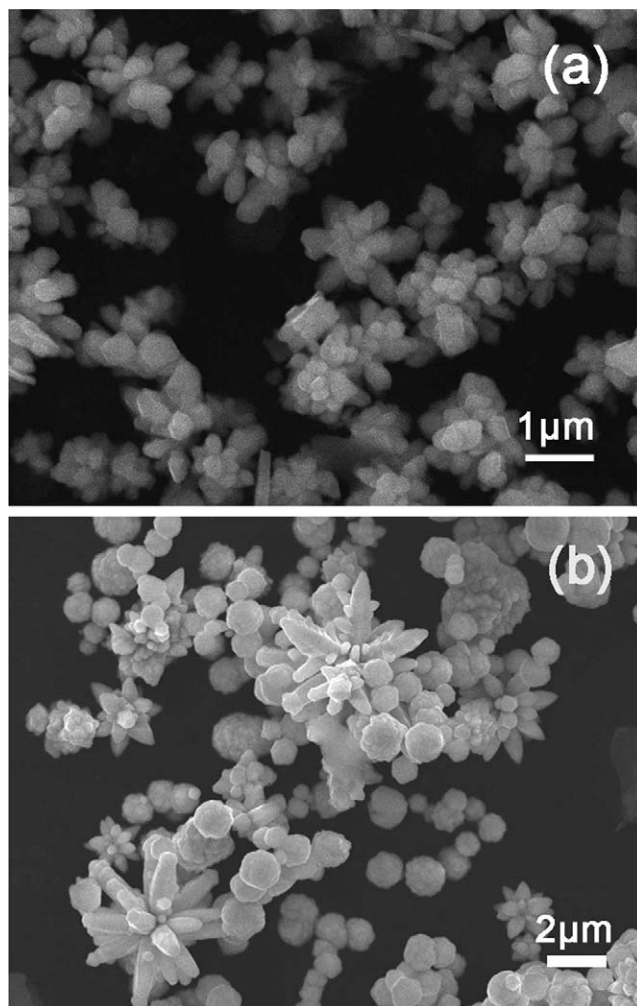


Fig. 4. SEM images of the samples prepared at 120 °C for 8 h in the absence (a) and 0.5 g (b) of sodium citrate.

favor of oriented growth [35]. Secondly, citrate ions can also serve as a shape modifier. At elevated temperature, the equilibrium constant for citrate ions binding to certain crystal faces of Co may change, leading to selective loss of citrate ions on certain crystal faces and allowing the particles to grow along one axis. Such a role of citrate has been also reported in the synthesis of large arrays of oriented ZnO nanostructures [36] and β -NiS 3D flowerlike architectures [37].

We also find that the concentration of NaOH is crucial to the formation of flowerlike Co. Contrast experiments have shown that the flowerlike structures were destroyed and spherical particle aggregations and short chains were formed, when the initial concentration of NaOH increased to 2 M keeping other parameters unchanged (Fig. 5a). When the concentration of NaOH was 3 M, only spherical particles with diameter of 0.3–1.8 μm were obtained (Fig. 5b), and no flowerlike structures were found. The magnified image shows that the surface of the spherical particles is quite rough (inset in Fig. 5b). Compared with those flowerlike structures observed in Fig. 1, these differences in the morphologies should be attributed to the reaction kinetics. It can be concluded that the higher concentration of NaOH restricted the growth of the flowerlike Co microcrystals. Chai et al. reported a similar result in the synthesis of $\text{La}_{0.5}\text{Ba}_{0.5}\text{MnO}_3$ products with different morphologies (flowerlike, microcube, and nanocube structures) by adjusting the alkalinity of the reaction solution [38]. When ammonia

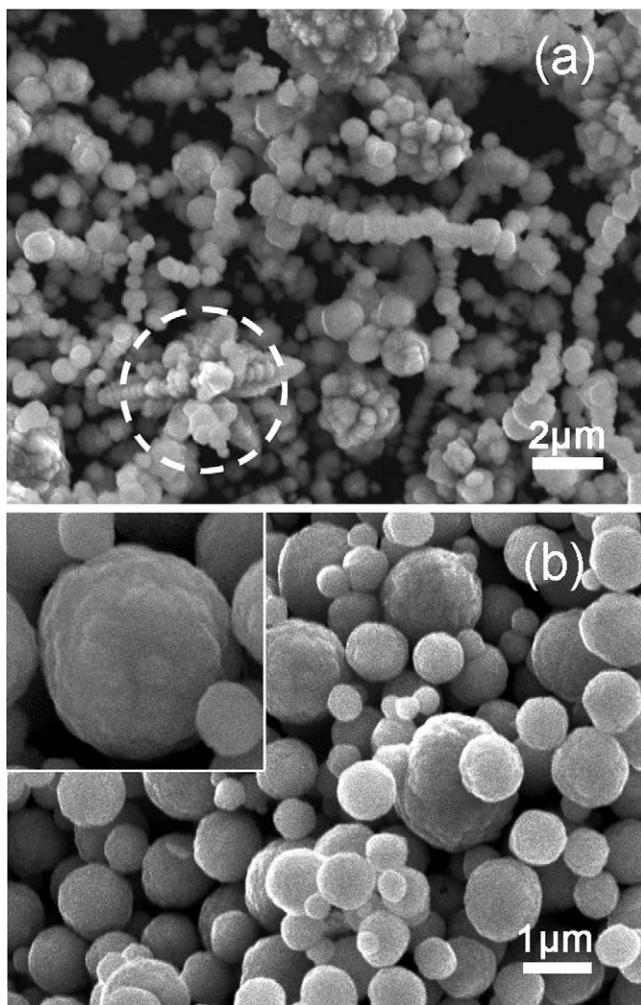


Fig. 5. SEM images of the samples prepared using different concentration of NaOH solution: (a) 2 M, (b) 3 M. The inset in (b) is a magnified image of single spherical particle.

$(\text{NH}_3 \cdot \text{H}_2\text{O})$ was used to tune the pH value of the solution instead of NaOH, no precipitations was found after hydrothermal treatment at 120 °C even if the reaction time was prolonged to 16 h. We have varied $\text{NH}_3 \cdot \text{H}_2\text{O}$ solution with different concentration, such as 5%, 15%, and 25% (v/v). No obviously difference was observed. The dissimilarity is likely related to the presence of NH_4^+ ions. It is well known that NH_4^+ ions could coordinate with Co^{2+} ions to form $[\text{Co}(\text{NH}_3)_6]^{2+}$ ions, which are more stable than $[\text{Co}(\text{C}_6\text{H}_5\text{O}_7)_2]^{4-}$ ions. Therefore, no Co could be formed at our reaction conditions. Thus, the choice of alkali is also a key factor for the formation of flowerlike Co structures.

To further investigate the morphological evolution process of flowerlike Co microcrystals, a series of experiments were carried out at different reaction durations (2, 4 and 8 h) while other parameters remained unchanged. Fig. 6a is the overall SEM image of products obtained at 120 °C for 2 h, which indicates only spherical particles with size of about 1 μm were obtained. The magnified image shows that each sphere was formed by assembly of smaller particles. When the hydrothermal time was prolonged to 4 h, a few flowerlike particles (marked by arrows in Fig. 6c) were found among the products. The petals of the flowerlike crystal are shorter (Fig. 6d), indicating the growth of the crystal is still incomplete. However, when the reaction time was further prolonged to 8 h, well-defined flowerlike Co crystals with high yield were obtained (Fig. 1).

In the light of the above experiment results, a possible growth mechanism is proposed. The schematic illustration of the formation mechanism of Co flowerlike structure is shown in Fig. 7. At the early stage of reaction, many nanoparticles with different sizes appeared in the solution (Fig. 7a). Because of the interaction between citrate ions binding to nanoparticles by van der Waals forces and intermolecular hydrogen bonds, Co nanoparticles would be assembled together (Fig. 7b). With the reaction proceeding continuously, assembled nanoparticles with a relatively large size might serve as the crystal nuclei. Due to the solvation of the Co surface, including hydrogen bonding, ion-dipole, and dipole-dipole interactions in polar solvents, thermodynamically active sites such as surface defects and active crystal surfaces were generated on the early formed Co nuclei. These active sites could then serve as heterogeneous nucleation sites. Once nuclei were formed at these active sites, the preferential orientation growth started. The preferential orientation of hcp Co in our reaction system was along the $[001]$ directions while citrate ions were used as shape modifier. As a consequence, many projecting petals could develop into a complex flowerlike 3D assembly sharing the same core. When the reactants were consumed due to particle growth, Ostwald ripening process occurred, where the larger particles continued to grow, and the smaller ones got smaller and finally dissolved (from Fig. 7b and c) [39]. It was reported that the morphology and size of the products depended on the competition between crystal nucleation and crystal growth, and the pH value had an impact on both the rate of crystal nucleation and the rate of crystal growth [38]. In our reaction system, with a low concentration of NaOH, namely, a low pH value, the crystal nucleation was slower than the crystal growth, which led to the formation of flowerlike structures with relatively larger size. While with a high concentration of NaOH, namely, a high pH value, the crystal nucleation was faster than the crystal growth. Therefore, the spherical structures with smaller size were obtained.

The magnetic hysteresis measurements of the as-synthesized Co structures were carried out at room temperature in the applied magnetic field sweeping from -15 to 15 kOe. Here we have chosen the flowerlike Co (corresponding to products shown in Fig. 1) and the spherical Co (corresponding to products shown in Fig. 5b) as examples to study the magnetic properties of Co microcrystals.

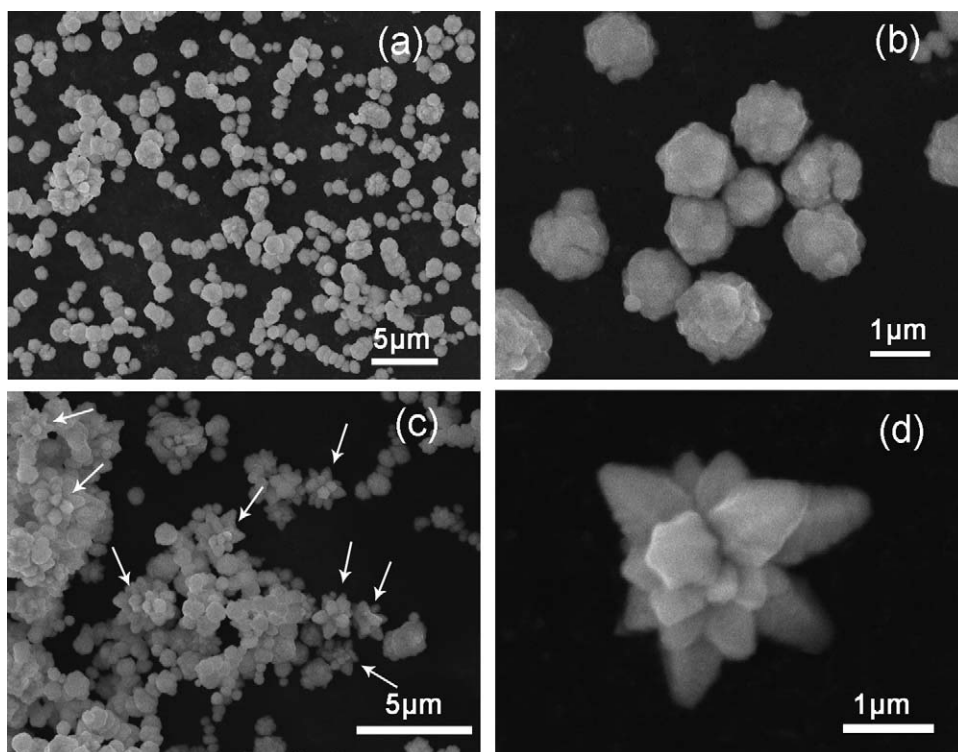


Fig. 6. SEM images of the samples prepared at 120 °C with different hydrothermal time of 2 h (a and b) and 4 h (c and d) respectively.

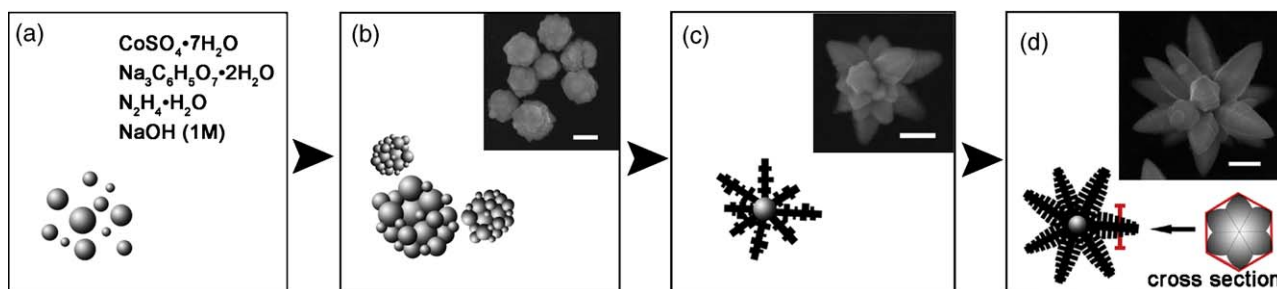


Fig. 7. Schematic illustration of the formation process of the flowerlike metallic Co microstructures: from (a) to (b) is the assembly process; from (b) to (d) is the typical Ostwald ripening process. The insets show SEM images of samples collected after hydrothermal treatment for 2, 4 and 8 h, respectively. The scale bars in all the insets represent 1 μm .

Both representative hysteresis loops of the as-synthesized flowerlike and spherical Co microcrystals are shown in Fig. 8, which demonstrate typical ferromagnetic behaviour. The saturation magnetization value (M_s) of the flowerlike Co is 128.1 emu/g, and the coercivity value (H_c) is 232.5 Oe. Meanwhile, the M_s of the spherical Co is 148.7 emu/g, and the H_c is 118.6 Oe. Both M_s of Co samples are much lower than that of bulk Co (168 emu/g) [40], which is attributed to the surface oxidation [40,41]. The flowerlike Co microcrystals exhibit a distinct enhanced coercivity compared with the value of spherical Co and bulk Co (a few tens of Oersteds at room temperature [16]). It is well known that magnetic properties of most materials are strongly affected by some type of anisotropy including crystal anisotropy, shape anisotropy, stress anisotropy, externally induced anisotropy, and exchange anisotropy [42]. The two most common anisotropies in micro-/nanostructured materials are crystalline and shape anisotropy. For flowerlike Co, its hcp phase, determined in the XRD pattern, would show higher coercivity owing to its relatively large crystal anisotropy constant. Furthermore, shape anisotropy is predicted to produce the largest coercive forces and even a small departure from sphericity in shape would result in the significant increase of coercivity [43]. Based on

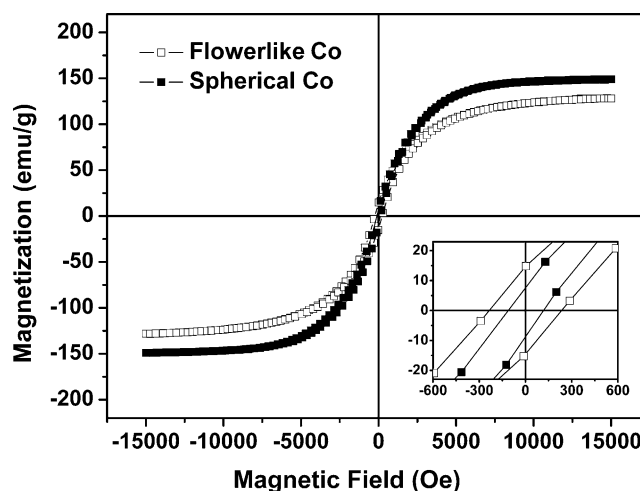


Fig. 8. Magnetic hysteresis loops for the synthesized samples: flowerlike Co microcrystals and spherical Co microcrystals. The inset shows the low-field part of the hysteresis loops.

the above discussion, the high coercivity of the synthesized flowerlike Co microcrystals should be attributed to the anisotropic shape and the hcp crystal structure.

4. Conclusions

In summary, well-defined, 3D flowerlike metallic Co microcrystals have been successfully synthesized via a facile hydrothermal reduction route. The unique flowery structures composed by hexagonal-tapered petals are reported for the first time. The morphology of the Co microcrystals can be controlled from flowerlike Co to spherical Co by changing the concentration of NaOH. A possible formation mechanism of the crystal was proposed on the basis of the experimental results. The synthesized flowerlike products exhibited a ferromagnetic nature with a significant enhanced magnetic coercivity due to the anisotropic shape and the hcp crystal structure. These special microcrystals may process promising application in microdevices. What is more, we believe that this method may provide a facile strategy to fabricate complex hierarchical structures.

Acknowledgments

This work was supported by Shanghai Nanotechnology Promotion Center (0852nm03200), the PhD Program Scholarship Fund of ECNU 2008 (Grant 20080045) and Equipment Sharing Platform of ECNU.

References

- [1] G.M. Whitesides, B. Grzybowski, *Science* 295 (2002) 2418–2421.
- [2] Z.L. Wang, *Adv. Mater.* 10 (1998) 13–30.
- [3] P.V. Kamat, *J. Phys. Chem. B* 106 (2002) 7729–7744.
- [4] Z.L. Wang, Z. Dai, S. Sun, *Adv. Mater.* 12 (2002) 1944–1946.
- [5] P. Gambardella, S. Rusponi, M. Veronese, S.S. Dhesi, C. Grazioli, A. Dallmeyer, I. Cabria, R. Zeller, P.H. Dederichs, K. Kern, C. Carbone, H. Brune, *Science* 300 (2003) 1130–1133.
- [6] C.T. Black, C.B. Murray, R.L. Sandstrom, S. Sun, *Science* 290 (2000) 1131–1134.
- [7] K.T. Nam, D.W. Kim, P.J. Yoo, C.Y. Chiang, N. Meethong, P.T. Hammond, Y. Chiang, A.M. Belcher, *Science* 312 (2006) 885–888.
- [8] Azarian, A.I. Zad, A. Dolati, *Opt. Commun.* 274 (2007) 471–476.
- [9] J. Li, J. Huang, Y. Qin, F. Ma, *Mater. Sci. Eng. B* 138 (2007) 199–204.
- [10] L.L. Welbes, R.C. Scarrow, A.S. Borovik, *Chem. Commun.* 22 (2004) 2544–2545.
- [11] M. Aslam, R. Bhobe, N. Alem, S. Donthu, V.P. Dravid, *J. Appl. Phys.* 98 (2005) 074311.
- [12] P.K. Tyagi, A. Misra, M.K. Singh, D.S. Misra, J. Ghatak, P.V. Satyam, F. Le Normand, *Appl. Phys. Lett.* 86 (2005) 253110.
- [13] Y.J. Zhang, S. Ma, D. Li, Z.H. Wang, Z.D. Zhang, *Mater. Res. Bull.* 43 (2008) 1957–1965.
- [14] L. Guo, F. Liang, X. Wen, S. Yang, L. He, W. Zheng, C. Chen, Q. Zhong, *Adv. Funct. Mater.* 17 (2007) 425–430.
- [15] B.Q. Xie, Y. Qian, S. Zhang, S. Fu, W. Yu, *Eur. J. Inorg. Chem.* 2006 (2006) 2454–2459.
- [16] H. Cao, Z. Xu, H. Sang, D. Sheng, C. Tie, *Adv. Mater.* 13 (2001) 121–123.
- [17] Q. Xie, Z. Dai, W.W. Huang, J.B. Liang, C.L. Jiang, Y.T. Qian, *Nanotechnology* 16 (2005) 2958–2962.
- [18] F.T. Huanga, R.S. Liua, S.F. Hu, J. Magn. Mater. 304 (2006) e19–e21.
- [19] M.H. Pan, H. Liu, J.Z. Wang, J.F. Jia, X.Q.K. Xue, J.L. Li, S. Qin, U.M. Mirsaidov, X.R. Wang, J.T. Markert, Z. Zhang, C.K. Shih, *Nano Lett.* 5 (2005) 87–90.
- [20] K. Nielsch, F.J. Castañón, C.A. Ross, R. Krishnan, *J. Appl. Phys.* 98 (2005) 034318.
- [21] L.P. Zhu, H.M. Xiao, W.D. Zhang, Y. Yang, S.Y. Fu, *Cryst. Growth Des.* 8 (2008) 1113–1118.
- [22] R. Xu, T. Xie, Y. Zhao, Y. Li, *Cryst. Growth Des.* 7 (2007) 1904–1911.
- [23] W. He, P. Gao, L. Chu, L. Yin, Z. Li, Y. Xie, *Nanotechnology* 17 (2006) 3512–3517.
- [24] V.F. Puentes, K.M. Krishnan, A.P. Alivisatos, *Science* 291 (2001) 2115–2117.
- [25] Y. Zhu, H. Zheng, Q. Yang, A. Pan, Z. Yang, Y. Qian, *J. Cryst. Growth* 260 (2004) 427–434.
- [26] Y.L. Hou, H. Kondoh, T. Ohta, *Chem. Mater.* 17 (2005) 3994–3996.
- [27] C. Petit, A. Taleb, M.P. Pileni, *Adv. Mater.* 10 (2006) 259–261.
- [28] X. Liu, R. Yi, Y. Wang, G. Qiu, N. Zhang, X. Li, *J. Phys. Chem. C* 111 (2007) 163–167.
- [29] H. Li, S. Liao, *J. Phys. D: Appl. Phys.* 41 (2008) 1–7.
- [30] H.T. Yang, Y.K. Su, C.M. Shen, T.Z. Yang, H.J. Gao, *Surf. Interf. Anal.* 36 (2004) 155–160.
- [31] V. Fleury, *Nature* 390 (1997) 145–148.
- [32] D. Wang, C.M. Lieber, *Nat. Mater.* 2 (2003) 355–356.
- [33] L. Manna, D.J. Milliron, A. Meisel, E.C. Scher, A.P. Alivisatos, *Nat. Mater.* 2 (2003) 382–385.
- [34] Q. Liao, R. Tannenbaum, Z.L. Wang, *J. Phys. Chem. B* 110 (2005) 14262–14265.
- [35] Z. Liu, S. Li, Y. Yang, S. Peng, Z. Hu, Y. Qian, *Adv. Mater.* 15 (2003) 1946–1948.
- [36] Z.R. Tian, J.A. Voigt, J. Liu, B. Mckenzie, M.J. Mcdermott, M.A. Rodriguez, H. Konishi, H. Xu, *Nat. Mater.* 2 (2003) 821–826.
- [37] H. Li, L. Chai, X. Wang, X. Wu, G. Xi, Y. Liu, Y. Qian, *J. Cryst. Growth* 7 (2007) 1918–1922.
- [38] P. Chai, X. Liu, Z. Wang, M. Lu, X. Cao, J. Meng, *Cryst. Growth Des.* 7 (2007) 2568–2575.
- [39] C. Burda, X. Chen, R. Narayanan, M.A. El-Sayed, *Chem. Rev.* 105 (2005) 1025–1102.
- [40] G. Dumpich, T.P. Krome, B. Hausmanns, *J. Magn. Mater.* 248 (2002) 241–247.
- [41] B. Hausmanns, T.P. Krome, G. Dumpich, *J. Appl. Phys.* 93 (2003) 8095–8097.
- [42] B.D. Cullity, *Introduction to Magnetic Materials*, Addison-Wesley Publishing Company, Reading, MA, 1972, pp. 240–243.
- [43] D.L. Leslie-Pelecky, R.D. Rieke, *Chem. Mater.* 8 (1996) 1770–1783.